NASA TECHNICAL MEMORANDUM

NASA TM X-1895

NASA TM X-1895

FLIGHT-MEASURED AERODYNAMIC DRAG OF TWO LARGE EXTERNAL TANKS ATTACHED TO THE X-15-2 AIRPLANE AT MACH NUMBERS OF 1.6 TO 2.3

by David F. Fisher

Flight Research Center
Edwards, Calif.

NATIONAL AERONAUTICS AND SPACE ADMINISTRATION • WASHINGTON, D. C. • OCTOBER 1969

1. Report No. NASA TM X-1895	2. Government Accession No.	3. Recipient's Catalog No.
4. Title and Subtitle FLIGHT-MEASURED AERODYNAMIC DRAG OF TWO LARGE EXTERNAL TANKS ATTACHED TO THE X-15-2 AIRPLANE AT MACH NUMBERS OF 1.6 TO 2.3		5. Report Date October 1969 6. Performing Organization Code
7. Author(s) David F. Fisher		8. Performing Organization Report No. H-564 10. Work Unit No. 722-51-00-01-24
9. Performing Organization Name and Address NASA Flight Research Center P. O. Box 273 Edwards, Calif. 93523		11. Contract or Grant No. 13. Type of Report and Period Covered Technical Memorandum
12. Sponsoring Agency Name and Address National Aeronautics and Space Administration Washington, D. C. 20546		14. Sponsoring Agency Code

15. Supplementary Notes

16. Abstract

Full-scale power-on flight lift and drag measurements were made on the X-15-2 airplane just before and just after two large external fuel tanks were ejected. By subtracting the drag of the airplane after tank ejection from the drag of the airplane before tank ejection, the incremental drag due to the tanks was determined.

Analysis of the data showed that the percentage increase of incremental drag due to the tanks was almost equal to the percentage increase in cross-sectional area caused by the tanks. A buildup drag estimate based on free-stream conditions agreed well with the flight data; whereas, the wind-tunnel data, although they had the same general trend of tank drag coefficient with Mach number, were lower than both the estimate and the flight data.

17. Key Words Suggested by Author(s)	18. Distribution Statement
X-15-2 airplane - External tank drag - Store drag	Unclassified - Unlimited

19. Security Classif. (of this report)	20. Security Classif. (of this page)	21. No. of Pages	22. Price *
Unclassified	Unclassified	14	$3.00

*For sale by the Clearinghouse for Federal Scientific and Technical Information, Springfield, Virginia 22151.

FLIGHT-MEASURED AERODYNAMIC DRAG OF TWO LARGE EXTERNAL TANKS ATTACHED TO THE X-15-2 AIRPLANE AT MACH NUMBERS OF 1.6 TO 2.3

By David F. Fisher
Flight Research Center

INTRODUCTION

Although numerous experiments have been performed to define the aerodynamic characteristics of external stores (ref. 1), little of this data defines the incremental drag due to the stores. Hoerner has compiled some store drag data in reference 2, but this compilation is limited to subscale models and subsonic velocities. One full-scale flight evaluation of the external-store drag increment is described in reference 3, but this is restricted to subsonic speeds. In another experiment of interest, a 1/7-scale model of a large store was tested in flight to Mach 2.45 by the National Advisory Committee for Aeronautics. In this test (results unpublished), however, the store was not in the presence of an airplane.

It is apparent that there is a general lack of full-scale drag data for external stores, particularly at supersonic speeds, and for stores which are large relative to the parent airplane. Therefore, the drag increment of two large external tanks attached to the X-15 airplane should be of value to aircraft and launch-vehicle designers.

The external tanks (one for fuel and one for liquid oxygen) were added to the X-15-2 airplane to provide extra propellants when flights above a Mach number of 6 were planned. These tanks were depleted of propellant before the primary internal tanks and were ejected when empty, near Mach 2. Thus, determining vehicle drag prior to and almost immediately after tank ejection provides a convenient way of defining the drag increment due to the tanks for a given condition during one flight.

The data presented herein, from four flights of the X-15-2 airplane, were obtained at Mach numbers of 1.6 to 2.3. The angle of attack varied from -2.0° to 6.5°, the dynamic pressure ranged from 288 lb/ft^2 (13,790 N/m^2) to 618 lb/ft^2 (29,590 N/m^2), and the Reynolds number based on tank length varied from 1.97×10^7 to 6.56×10^7.

Flight data are compared with wind-tunnel data from X-15-2 models and with data obtained by using a drag buildup prediction method.

SYMBOLS

The units used for the physical quantities in this paper are given in U.S. Customary Units and parenthetically in the International System of Units (SI). Factors relating the two systems are presented in reference 4.

A	base cross-sectional area of each external tank, 7.77 ft^2 (0.722 m^2)
A_e	exit area of rocket engine, 4.01 ft^2 (0.373 m^2)
A_t	throat area of rocket engine, 0.4095 ft^2 (0.0380 m^2)
a_l	longitudinal acceleration along body axis
a_n	acceleration (load factor) normal to body axis
C_D	drag coefficient of airplane with and without tanks, $\frac{Drag}{qS}$
C_f	thrust coefficient of rocket engine
C_L	lift coefficient of airplane with and without tanks, $\frac{Lift}{qS}$
g	acceleration due to gravity, ft/sec^2 (m/sec^2)
M	Mach number
p_c	chamber pressure of rocket engine, lb/ft^2 (N/m^2)
p_e	exit pressure of rocket engine, lb/ft^2 (N/m^2)
p_∞	ambient pressure, lb/ft^2 (N/m^2)
q	dynamic pressure, lb/ft^2 (N/m^2)
S	reference area of wing, 200 ft^2 (18.6 m^2)
T	thrust of rocket engine, lb (N)
W	weight of airplane, lb (kg)
α	angle of attack, deg
ΔC_{D_t}	increment of drag coefficient attributable to the tanks, C_{D_o} with tanks minus C_{D_o} without tanks
$\Delta C_{D_t}'$	increment of drag coefficient attributable to the tanks based on the cross-sectional area of the two tanks, $\frac{\Delta C_{D_t} S}{2A}$

Subscript:

o at zero lift coefficient

AIRPLANE

The X-15 is a single-place, low-aspect-ratio monoplane originally designed for manned flight research to about Mach 6. A general description of the airplane and its functions is presented in reference 5. The X-15 was subsequently modified to extend its Mach number range to near Mach 8 and was designated X-15-2. A three-view drawing of the X-15-2 is shown in figure 1, and physical characteristics are given in

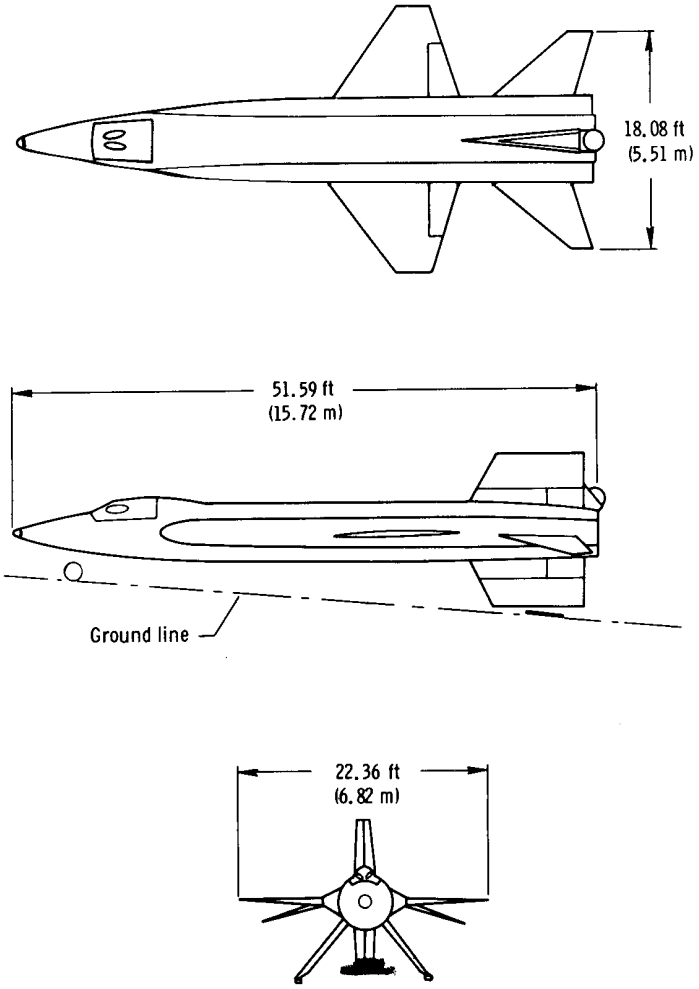

Figure 1.– Three-view drawing of X-15-2 airplane.

table I. The primary modification was the addition of two large external tanks, shown attached to the airplane in figures 2(a) and 2(b). This configuration was flown for three of the four flights discussed in this report. For the fourth flight, the X-15-2 was

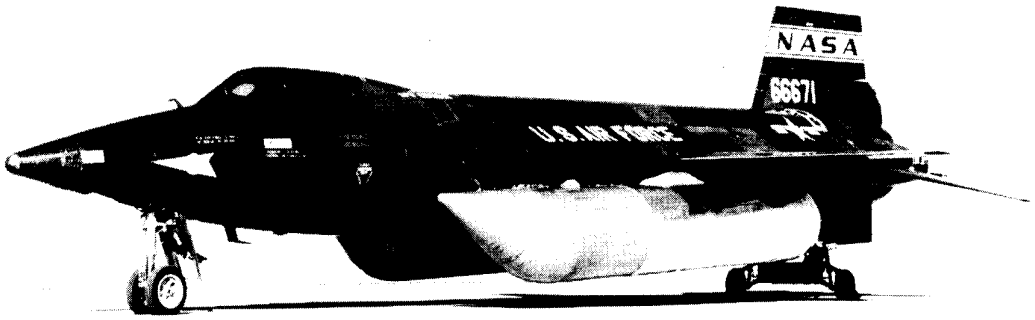

(a) Side view. E-13888

(b) Front view. E-13890

Figure 2.– X-15-2 with external tanks (two-wheeled dolly supporting rear of airplane not part of airplane).

equipped with the two tanks; in addition, it was coated with an ablative material, and a dummy ramjet was mounted on a modified lower vertical tail. This configuration is shown in figure 3. Other pertinent modifications included the following:

1. Fuselage extended 29 inches (74 centimeters) by an insert at the wing, moving the nose forward but keeping the same wing-tail relationship.

2. Fuselage and fuel system modified to support, utilize, and eject the two external tanks.

3. Landing gears strengthened and lengthened.

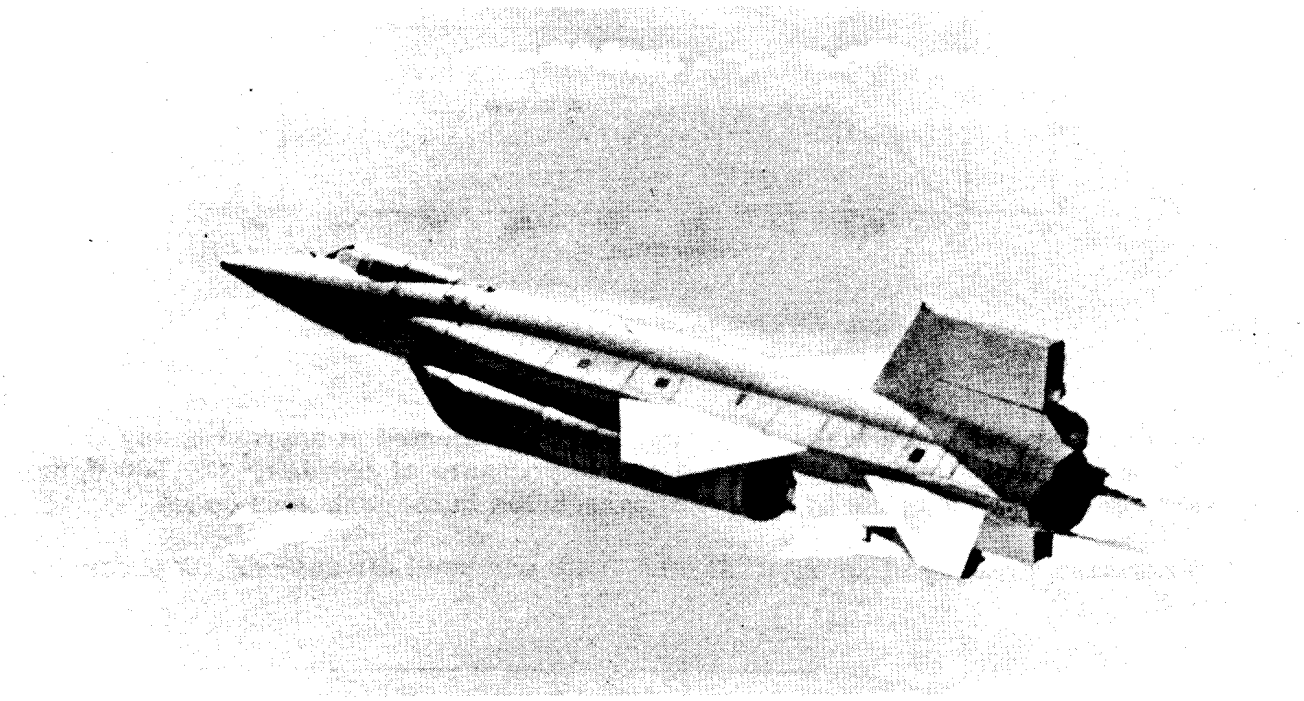

Figure 3.– X-15-2 in flight with external fuel tanks, ablative coating, and dummy ramjet.

The most important physical change, insofar as drag is concerned, is the additional cross-sectional area of the airplane-tank configuration. The cross-sectional-area distribution of the X-15-2 with and without the external tanks is shown as a function of fuselage station in figure 4.

The external tanks, which were cylindrical with blunted 40° conical noses and hemispherical bases, were attached to the airplane with pylons. The noses were canted to help fair them into the airplane body and reduce drag. A 0.5-inch- (1.27-centimeter-) thick insulation was placed on the outside of the left external tank starting about 112 inches (284 centimeters) from the nose and extending to and covering the base. It was faired smoothly to the tanks at the front and was continuous at the base. The increase in cross-sectional area resulting from this insulation was determined to have a negligible effect on the results and was thus neglected in all calculations.

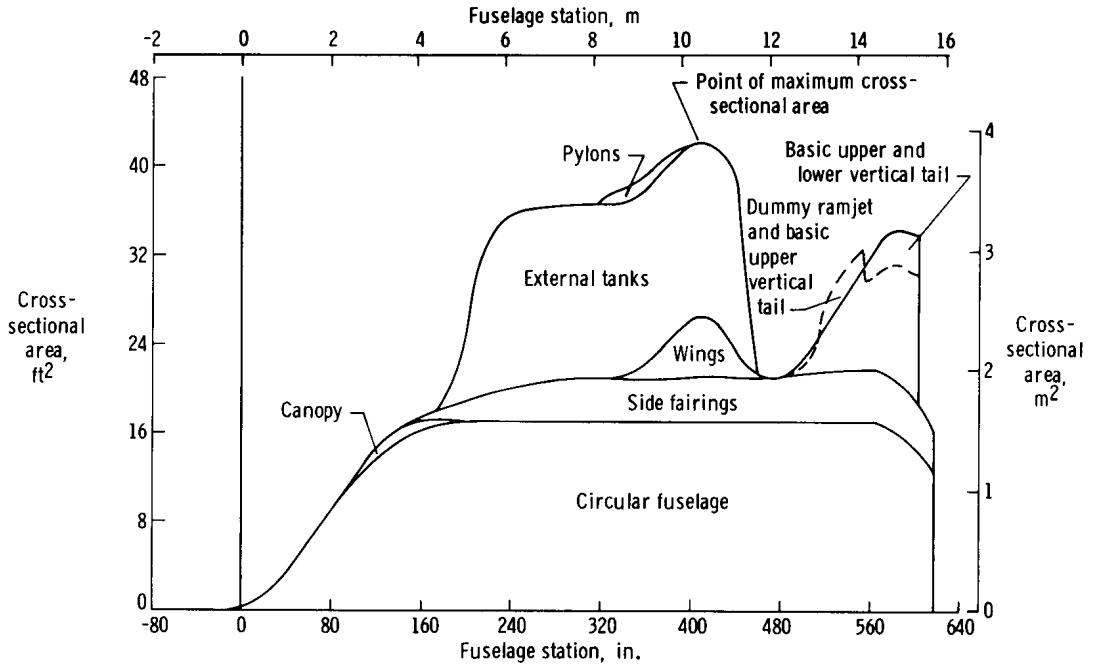

Figure 4.– Cross-sectional-area distribution.

After being emptied, the tanks were designed to be ejected at approximately Mach 2.2, an angle of attack of 5°, and a dynamic pressure of 300 lb/ft^2 (14,500 N/m^2). They were recovered for reuse by means of parachutes in the tank nose cones.

A three-view drawing of an external tank, with pertinent dimensions, is presented in figure 5.

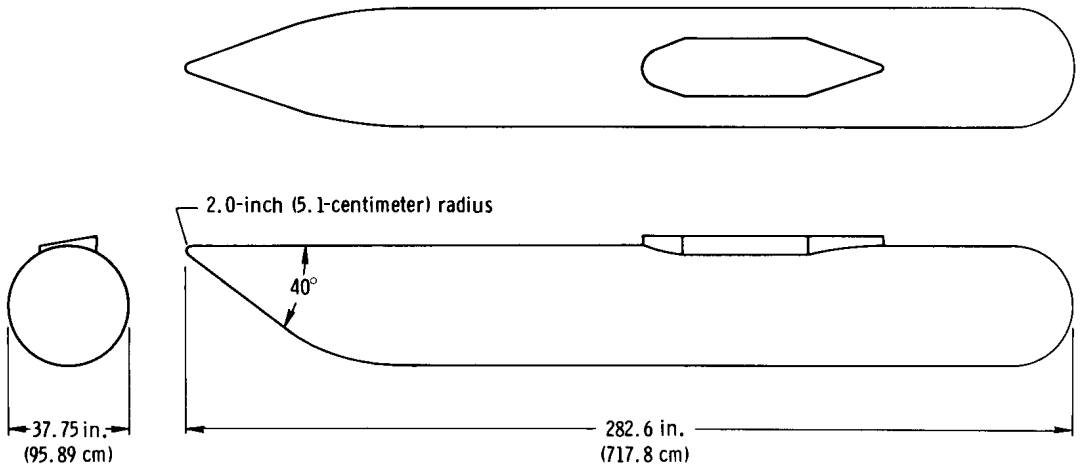

Figure 5.– Three-view drawing of external fuel tank.

INSTRUMENTATION

For all four flights, NACA internal recording instruments were used to measure longitudinal and normal accelerations and chamber pressure (ref. 6). However, on flights 43, 50, and 53 (see table, page 8), the longitudinal acceleration exceeded the range of the ±1 g NACA accelerometer unit installed in the airplane. For these flights an auxiliary strain-gage type of longitudinal accelerometer was used: a ±5g accelerometer for flights 43 and 50, and a ±2g accelerometer for flight 53. The accelerometers were positioned as close to the airplane center of gravity as possible to minimize error due to displacement.

Angle of attack and angle of sideslip were measured by a spherical flow-direction sensor (ref. 7). Mach number and ambient pressure were determined with radiosonde balloons and radar tracking. The method used to determine Mach number and static pressure from which dynamic pressure is derived is discussed in references 8 and 9.

METHOD

Drag Determination

The accelerometer method (ref. 6) was used to determine the lift and drag of the airplane. The data points that were used in the calculations were those obtained immediately before and immediately after tank ejection after the high-frequency transients had subsided, which was usually within 2 seconds. Thus, by subtracting the drag of the airplane after tank ejection from the drag of the airplane before tank ejection, the incremental drag due to the tanks was determined. For all flights the airplane was accelerating at the time of tank ejection. For one of these flights, however, a longer transient condition existed following tank ejection, which required a small correction in drag coefficient C_D to compensate for the change in Mach number with time.

For power-on conditions, the relationships used to calculate lift coefficient C_L and drag coefficient C_D were as follows:

$$C_D = \left(\frac{T - Wa_l}{qS}\right) \cos \alpha + \left(\frac{Wa_n}{qS}\right) \sin \alpha$$

$$C_L = \left(\frac{Wa_n}{qS}\right) \cos \alpha - \left(\frac{T - Wa_l}{qS}\right) \sin \alpha$$

Aircraft weight was determined by integrating the fuel flow rates, which are a known function of the measured chamber pressure, and subtracting these values from the known "full tanks" weight.

For the rocket engine, the thrust was determined by using the relationship from references 6 and 10 shown on the next page.

$$T = C_f A_t p_c + (p_e - p_\infty)A_e$$

The thrust coefficient C_f varied between 1.54 and 1.63, chamber pressure p_c was measured with a photomanometer, and ambient pressure p_∞ was determined from dynamic pressure and Mach number. For a specific-heat ratio of 1.23 and an area ratio of 9.8 for the rocket engine, the exit pressure p_e equals $p_c/85$, assuming isentropic flow.

Drag Prediction

The estimated tank drag-coefficient increment, based on free-stream Mach number and zero angle of attack, was built up as follows:

$$\Delta C_{D_t} = C_{D_{(\text{hemispherical nose})}} + C_{D_{(\text{pylon})}} + C_{D_{(\text{canted cone})}} + C_{D_{\text{base}}} + C_{D_{\text{friction}}}$$

The drag of the hemispherical nose and pylon was determined from reference 2. The cone drag $\left(C_{D_{(\text{canted cone})}}\right)$ was calculated by using the cone tables from reference 11 and information in reference 12. The base drag of the tanks was calculated by adjusting sphere base drag (ref. 2) for the appropriate length-diameter ratio of the tanks using figure 9, page 16-9, of reference 2. The turbulent skin-friction drag was derived from charts in reference 13.

This estimate neglects any effect of interference. Pressure gradients on the cylindrical portion of the tanks would have little influence on drag, since both the tanks and the adjacent fuselage were nearly parallel to each other and to the flight path. However, with tanks that have less-blunt noses and bases, i.e., sloping surfaces, this method may prove to be inadequate.

TEST CONDITIONS

The test conditions for the selected portions of the four flights discussed herein are summarized in the following table:

Flight number	M	q, lb/ft^2 (N/m^2)	Reynolds number based on tank length	W, lb (kg)		Nominal thrust at tank ejection, lb (N)
				Before tank ejection	After tank ejection	
43	2.25	343 (16,400)	2.36×10^7	25,350 (11,500)	23,500 (10,660)	36,000 (160,000)
45	1.62	618 (29,600)	6.56	43,900 (19,910)	36,500 (16,560)	35,000 (156,000)
50	2.27	342 (16,400)	2.46	37,100 (16,830)	35,200 (15,970)	60,000 (267,000)
53	2.20	288 (13,800)	1.97	37,700 (17,100)	35,800 (16,240)	60,000 (267,000)

Angle of attack varied at tank ejection from 3.5° to 6.5°. The altitude at tank ejection on flight 45 was about 41,900 feet (12,800 meters); on the other three flights it was approximately 70,000 feet (21,000 meters).

On flight 53, ablative material was applied to the skin of the aircraft, and the dummy ramjet was installed on a modified lower vertical tail. Because the increment of drag to be defined in this study is for the tanks only (no ablative was applied to the tanks), these configuration changes should have negligible effect on the results.

ERROR AND RELIABILITY

As mentioned in the METHOD section, the incremental tank drag was determined by subtracting the airplane drag after tank jettison from the airplane drag before tank jettison. This procedure eliminates first-order bias errors in the determination of tank drag coefficient. Fortunately in this instance, one of the largest sources of error in measuring airplane drag, the determination of thrust, is primarily a bias error. This error is principally in the measurement of p_c and the determination of C_f. Other bias errors are likewise minimized in their effect on tank drag coefficient; therefore, it is primarily random error which influences the measurement of tank drag.

Since different longitudinal accelerometers were used for the four flights, the random error should vary from flight to flight. The estimated error in C_D for the flights is as follows: flights 43 and 50, ±0.016; flight 45, ±0.004; and flight 53, ±0.008. An additional error, a random error in measuring thrust, is not included in these estimates. This error would be about ±0.002 and would not necessarily be additive to the estimated errors.

DISCUSSION OF RESULTS

Flight data are presented in the form of $C_L{}^2$ as a function of C_D in figures 6(a) to 6(d). In this manner, it is easier to extrapolate to the zero-lift drag, particularly

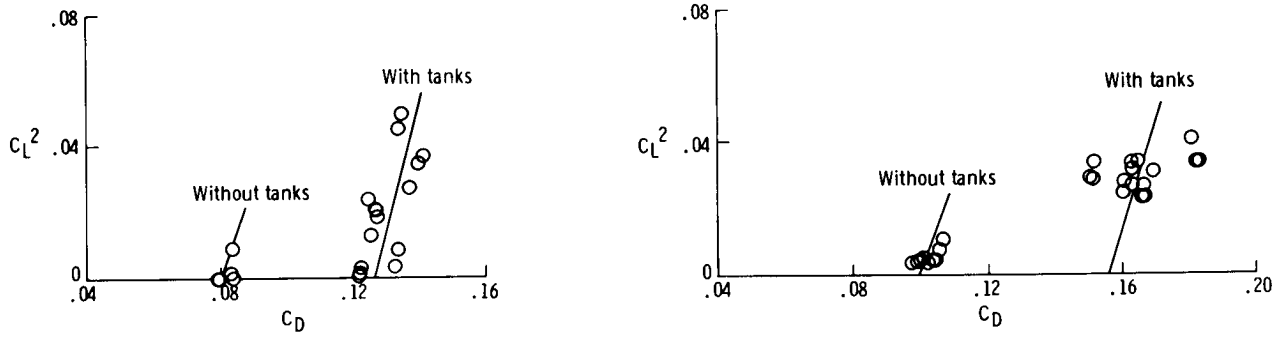

(a) Flight 43, Mach 2.25. *(b) Flight 50, Mach 2.27.*

Figure 6.– Variation of $C_L{}^2$ with C_D for the X-15-2 with and without tanks.

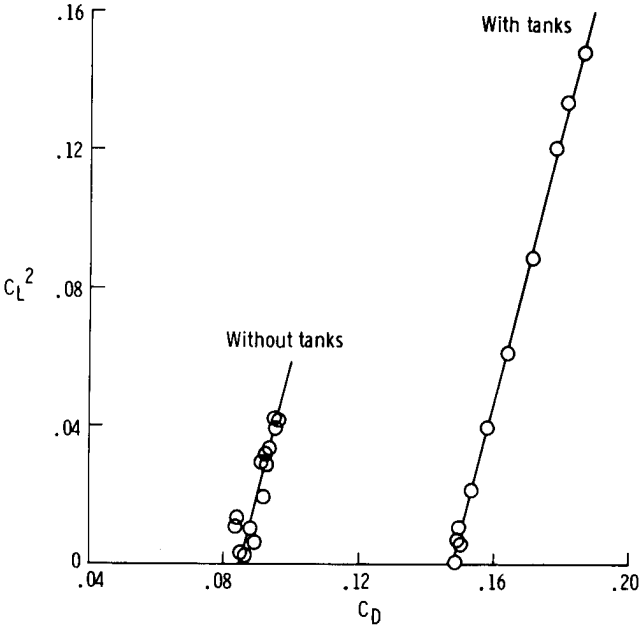

(c) Flight 45, Mach 1.62.

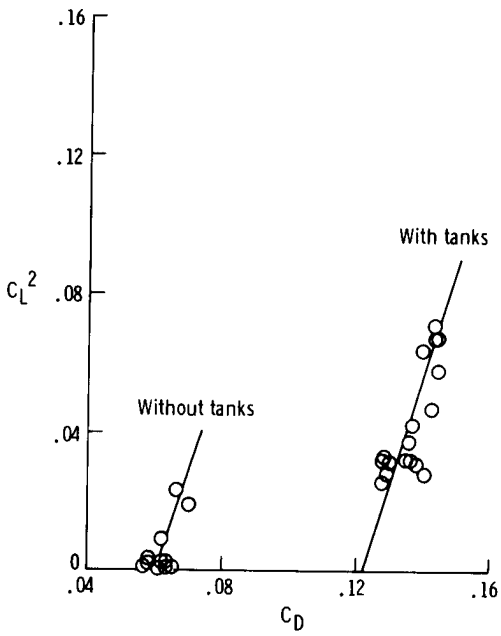

(d) Flight 53, Mach 2.20.

Figure 6.– Concluded.

when the segment of the drag polar does not reach zero-lift conditions. Although the absolute values of aircraft drag coefficient do not agree from flight to flight, because of previously mentioned bias errors in determining thrust, the incremental drag due to the tanks is valid because the thrust variation was small during the sampling interval for each flight.

The incremental zero-lift drag coefficient attributable to the tanks is shown in figures 7(a) and 7(b) as a function of Mach number. Dual ordinate scales are used: The scale labeled ΔC_{D_t} is referenced to the airplane wing area, and the scale labeled $\Delta C_{D_t'}$ is referenced to the cross-sectional area of the two tanks, which is the more conventional reference area for such bodies. (Here, reference area equals 2A because the measured increment of drag represents two tanks.) In figure 7(a) the flight-determined values of tank drag coefficient are presented along with the total predicted drag coefficient and the predicted component drag coefficients. In figure 7(b) included with the flight-determined values are wind-tunnel data from reference 14 and unpublished wind-tunnel results for the same configuration for tests conducted at the Jet Propulsion Laboratory, California Institute of Technology. Also included in figure 7(b) is the curve of predicted total drag coefficient from figure 7(a).

The estimated increment, based on well known and readily available references applied to free-stream conditions, appears to be a good fairing for the flight data. The wind-tunnel data of reference 14 show the same general trend of ΔC_{D_t} with Mach number, but are about 17 percent below the prediction and lower than the flight data. The wind-tunnel value from the Jet Propulsion Laboratory study shows better

agreement with the prediction and the flight results.

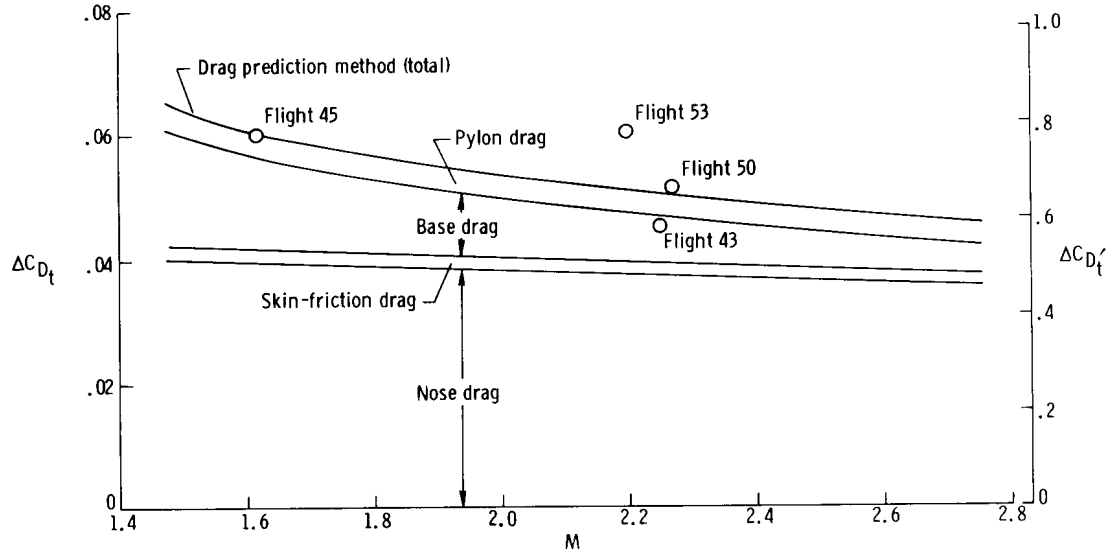

(a) Comparison of flight drag data with predicted total and tank component drag data.

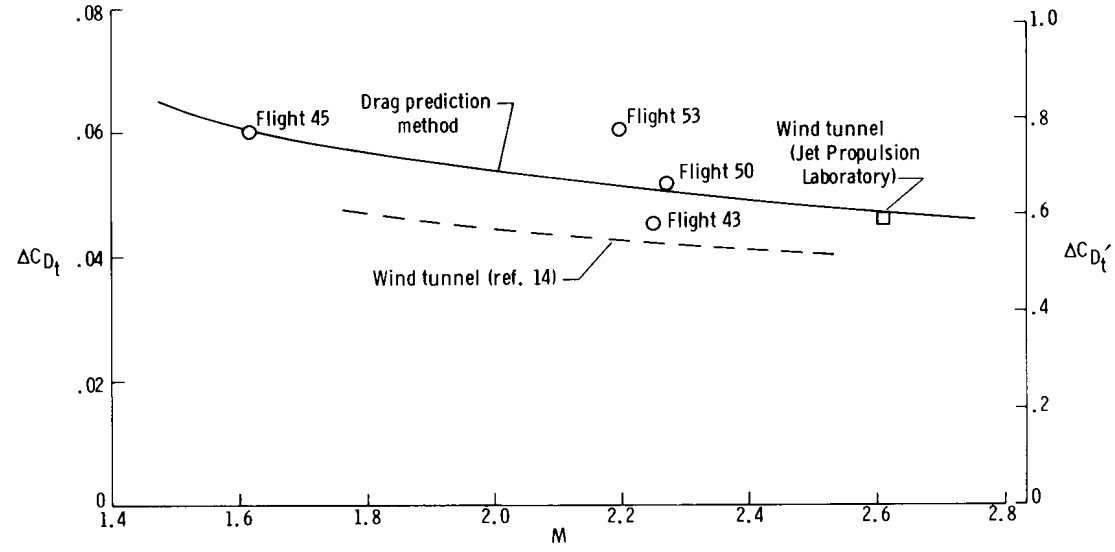

(b) Comparison of flight-determined and predicted drag data with wind-tunnel data.

Figure 7.– Variation of tank drag with Mach number at zero lift.

By using the zero-lift drag coefficients from reference 15 for the drag of the airplane without tanks, calculations were made to relate the tank-induced increase in drag to the increase in cross-sectional area. This relationship between area and drag is found to be rather direct. At the point of maximum cross-sectional area (fig. 4), the tanks represent 37 percent of the total area; whereas, at zero lift, the tank drag coefficient was 41 percent of the total drag coefficient between Mach numbers of 1.6 and 2.3.

CONCLUDING REMARKS

Flight incremental drag measurements were made on the external tanks of the X-15-2 airplane by subtracting the drag of the airplane after tank ejection from the drag of the airplane before tank ejection.

The results of this study at Mach numbers of 1.6 and 2.3 indicated that at zero-lift conditions, the increment of drag due to the tanks, as a percentage of the total drag, was almost equal to the increment of cross-sectional area of the tanks, as a percentage of the total maximum cross-sectional area. In addition, the buildup estimate of tank drag based on free-stream conditions agreed well with the flight results (having a similar magnitude and variation with Mach number) and, in effect, was a good fairing for the flight results. The most comparable wind-tunnel data, although 17 percent lower than the estimate, were consistent with the estimate in variation of tank drag coefficient with Mach number.

Flight Research Center,
National Aeronautics and Space Administration,
Edwards, Calif., July 18, 1969.

REFERENCES

1. McKinney, Linwood W.; and Polhamus, Edward C.: A Summary of NASA Data Relative to External-Store Separation Characteristics. NASA TN D-3582, 1966.

2. Hoerner, Sighard F.: Fluid-Dynamic Drag. Publ. by the author (148 Busteed Dr., Midland Park, N. J.), 1965.

3. Nugent, Jack: Effect of Wing-Mounted External Stores on the Lift and Drag of the Douglas D-558-II Research Airplane at Transonic Speeds. NACA RM H57E15a, 1957.

4. Mechtly, E. A.: The International System of Units. Physical Constants and Conversion Factors. NASA SP-7012, 1964.

5. Weil, Joseph: Review of the X-15 Program. NASA TN D-1278, 1962.

6. Beeler, De E.; Bellman, Donald R.; and Saltzman, Edwin J.: Flight Techniques for Determining Airplane Drag at High Mach Numbers. NACA TN 3821, 1956.

7. Wolowicz, Chester H.; and Gossett, Terrence D.: Operational and Performance Characteristics of the X-15 Spherical, Hypersonic Flow-Direction Sensor. NASA TN D-3070, 1965.

8. Larson, Terry J.; and Webb, Lannie D.: Calibrations and Comparisons of Pressure-Type Airspeed-Altitude Systems of the X-15 Airplane From Subsonic to High Supersonic Speeds. NASA TN D-1724, 1963.

9. Webb, Lannie D.: Characteristics and Use of X-15 Air-Data Sensors. NASA TN D-4597, 1968.

10. Sutton, George P.: Rocket Propulsion Elements. Second ed., John Wiley & Sons, Inc., 1956.

11. Staff of the Computing Section, Center of Analysis: Tables of Supersonic Flow Around Cones of Large Yaw. Tech. Rep. No. 5, Mass. Inst. Tech., 1949.

12. Van Dyke, Milton D.; Young, George B. W.; and Siska, Charles: Proper Use of the M. I. T. Tables for Supersonic Flow Past Inclined Cones. J. Aeron. Sci., vol. 18, no. 5, May 1951, pp. 355-356.

13. Bertram, Mitchel H.: Calculations of Compressible Average Turbulent Skin Friction. NASA TR R-123, 1962.

14. Graves, Ernald B.: Effect of Hypersonic Research Engine Installation on Aerodynamic Characteristics of 0.0667-Scale Model of X-15A-2 Airplane at Mach Numbers From 1.75 to 4.63. NASA TM X-1840, 1969.

15. Saltzman, Edwin J.; and Garringer, Darwin J.: Summary of Full-Scale Lift and Drag Characteristics of the X-15 Airplane. NASA TN D-3343, 1966.

TABLE I.– PHYSICAL CHARACTERISTICS OF THE X-15-2 AIRPLANE

Wing –	
Airfoil section	NACA 66005 (modified)
Total area (includes 94.98 ft^2 (8.82 m^2) covered by fuselage), ft^2 (m^2)	200 (18.6)
Span, ft (m)	22.36 (6.82)
Mean aerodynamic chord, ft (m)	10.27 (3.13)
Root chord, ft (m)	14.91 (4.54)
Tip chord, ft (m)	2.98 (0.91)
Taper ratio	0.20
Aspect ratio	2.50
Sweep at 25-percent-chord line, deg	25.64
Incidence, deg	0
Dihedral, deg	0
Aerodynamic twist, deg	0
Horizontal tail –	
Airfoil section	NACA 66005 (modified)
Total area (includes 63.29 ft^2 (5.88 m^2) covered by fuselage), ft^2 (m^2)	115.34 (10.7)
Span, ft (m)	18.08 (5.51)
Mean aerodynamic chord, ft (m)	7.05 (2.15)
Root chord, ft (m)	10.22 (3.12)
Tip chord, ft (m)	2.11 (0.64)
Taper ratio	0.21
Aspect ratio	2.83
Sweep at 25-percent-chord line, deg	45
Dihedral, deg	-15
Upper vertical tail –	
Airfoil section	10° single wedge
Total area, ft^2 (m^2)	40.91 (3.8)
Span, ft (m)	4.58 (1.40)
Mean aerodynamic chord, ft (m)	8.95 (2.73)
Root chord, ft (m)	10.21 (3.11)
Tip chord, ft (m)	7.56 (2.30)
Taper ratio	0.74
Aspect ratio	0.51
Sweep at 25-percent-chord line, deg	23.41
Lower vertical tail –	
Airfoil section	10° single wedge
Total area, ft^2 (m^2)	34.41 (3.2)
Span, ft (m)	3.83 (1.17)
Mean aerodynamic chord, ft (m)	9.17 (2.80)
Root chord, ft (m)	10.21 (3.11)
Tip chord, ft (m)	8 (2.44)
Taper ratio	0.78
Aspect ratio	0.43
Sweep at 25-percent-chord line, deg	23.41
Fuselage –	
Length, ft (m)	51.59 (15.72)
Maximum width, ft (m)	7.33 (2.23)
Maximum depth, ft (m)	4.67 (1.42)
Maximum depth over canopy, ft (m)	4.97 (1.51)
Side area (total), ft^2 (m^2)	221.38 (20.6)

NASA-Langley, 1969 —— 1 H-564